IOPscience

HOME | SEARCH | PACS & MSC | JOURNALS | ABOUT | CONTACT US

A multi-spectroscopic study of luminescence sensitivity changes in natural quartz induced by high-temperature annealing

This article has been downloaded from IOPscience. Please scroll down to see the full text article.

2001 J. Phys. D: Appl. Phys. 34 722

(http://iopscience.iop.org/0022-3727/34/5/310)

The Table of Contents and more related content is available

Download details:
IP Address: 138.251.105.135
The article was downloaded on 23/06/2009 at 12:15

Please note that terms and conditions apply.

INSTITUTE OF PHYSICS PUBLISHING JOURNAL OF PHYSICS D: APPLIED PHYSICS

J. Phys. D: Appl. Phys. **34** (2001) 722–731 www.iop.org/Journals/jd PII: S0022-3727(01)17190-1

A multi-spectroscopic study of luminescence sensitivity changes in natural quartz induced by high-temperature annealing

T Schilles[1], N R J Poolton[4], E Bulur[2], L Bøtter-Jensen[2], A S Murray[3], G M Smith[4], P C Riedi[4] and G A Wagner[1]

[1] Forschungsstelle Archäometrie, der Heidelberger Akademie der Wissenschaften, am Max-Planck-Institut für Kernphysik, Saupfercheckweg 1, D-69117 Heidelberg, Germany
[2] Risø National Laboratory, DK 4000 Roskilde, Denmark
[3] Nordic Laboratory for Luminescence Dating, Department of Earth Sciences, Aarhus University, Risø National Laboratory, DK 4000 Roskilde, Denmark
[4] School of Physics and Astronomy, University of St Andrews, North Haugh, St Andrews, Fife KY16 9SS, Scotland, UK

Received 18 September 2000

Abstract

The luminescence sensitivity of natural quartz is significantly enhanced if heated beyond the first and second crystal phase transitions, in the temperature range 500–1100 °C. This work employs a number of complementary spectroscopic methods to obtain a fuller understanding of the mechanisms of this sensitization process. Spectrally resolved radioluminescence is used to study the role played by hole trapping recombination sites. Linearly-modulated optically stimulated luminescence is used to probe a number of different optically active electron donor defects. Spectrally resolved thermoluminescence simultaneously monitors the processes of electron eviction from donor centres, and recombination at acceptor sites. Finally, high-frequency electron paramagnetic resonance is used to monitor changes in population and structure of defects present within the lattice, some of which partake (either directly or indirectly) in the emission processes of the samples. The work leads to the conclusion that luminescence is generally sensitized in quartz by the removal of oxygen vacancy E′ centres (which act either as non-radiative recombination centres, or as luminescence centres emitting in the deep UV, beyond the range of our instrumentation). In some samples, further luminescence enhancement is accompanied by heat induced creation of donor defects. The spectral results show that, not only is there competition between the acceptors for recombining electrons, but also that the emission undergoes significant thermal quenching at elevated temperatures. Comparison of the radioluminescence and thermoluminescence measurements enables the quenching energies of two emission bands (360, 470 nm) to be obtained directly.

1. Introduction

Quartz is an excellent material for use in environmental dosimetry, both because of its almost ubiquitous availability, and its desirable quality of trapping and storing charge over long periods of time. It finds use as a radiation dosimeter in both archaeological and geological dating applications, and for assessment of dose following man-made radiation exposure (e.g. Chernobyl, Hiroshima etc). Methods of accrued dose assessment include electron paramagnetic resonance (EPR),

 © 2001 IOP Publishing Ltd Printed in the UK

thermoluminescence (TL), optically stimulated luminescence (OSL) and radioluminescence (RL). These methods tend to be complementary, with each one particularly suited to different applications: examples include geological fault dating (EPR: Lee and Schwarcz 1994), water-lain or wind-blown sediment dating (OSL: Aitken 1998), archaeological pottery dating (TL: Aitken 1985), nuclear exposure assessment using house bricks (RL: Marazuev *et al* 1995).

Although the bulk structure of quartz used is normally the same regardless of its origin (usually α-quartz), the detailed dosimetric properties of the material depends upon the point defects contained within the crystal matrix. However, the defect type, structure and population can vary markedly from sample to sample. In studying the detailed TL emission spectra of a wide variety of quartz material, Rink *et al* (1993) concluded that broadly, the colour of the TL emission is indicative of the provenance, growth method and thermal history of the material. For example, material of volcanic origin is usually dominated by red (630 nm) emission; hydrothermal quartz is usually weakly emitting, mainly at 560–580 nm, and granitic quartz can have various emissions at 369–380 nm, 420–470 nm and at 630 nm. Many other investigations are generally in accord with these observations, and a recent review of this literature can be found in Krbetschek *et al* (1997).

Whereas for TL dosimetry a broad choice of emission wavelengths is available for analysis, the choice is more limited in the case of current wave (CW) OSL methods, due to the necessity of using excitation wavelengths in the blue/green spectral regions; in most systems, detection is limited to the range 300–380 nm. This is fortuitous, since in spectrally resolved OSL emission, the luminescence of several sedimentary samples has been shown to be dominated by an emission band peaking in the UV, at around 365 nm (Huntley *et al* 1991, 1996). However, luminescence detected in this region shows unusual characteristics. Bøtter-Jensen *et al* (1995) showed that in several different natural quartz sediments (and synthetic material) high-temperature annealing (0–1100 °C) prior to irradiation could significantly increase the sensitivity of the measurements, typically by three orders of magnitude: the sensitivity increase was found to normally occur between the first two phase transition temperatures (573 and 870 °C). In a more detailed study, Poolton *et al* (2000) attempted to correlate such OSL behaviour of material that had undergone successive annealing treatments, with changes in the defect structures and populations, as monitored by EPR. They tentatively concluded that oxygen vacancy (E') centres act as non-radiative recombination centres, competing with the trap responsible for the UV emission: such E' centres are annealed out of the samples at temperatures in the range 500–700 °C, explaining the OSL sensitivity increase. The conclusions could only be tentative, since no spectral information was available to analyse potential sensitivity changes occurring elsewhere in the emission spectrum.

The object of the work presented here is to make a more conclusive study of the origins of high-temperature anneal induced sensitivity changes that occur in natural sedimentary quartz, by undertaking a range of complementary spectral measurements on the *same* material. RL emission spectra are recorded to isolate and monitor the main changes in the recombination emission processes. Linearly modulated OSL (LM-OSL) is used to monitor changes in the OSL excitation process from a variety of optically active electron traps (see Bulur *et al* (2000) for method description). TL emission spectroscopy is used to monitor changes in the TL properties of the material. Finally, high-frequency EPR is used to monitor anneal induced changes in the population and structure of both electron and hole trapping paramagnetic centres present.

2. Experimental details

2.1. Equipment

Spectral measurements were carried out in Heidelberg using the TL/OSL-Spectrometer described by Rieser *et al* (1999). Here, a Czerny–Turner flat field spectrograph (Acton SP150) was equipped with a grating of 150 lines mm^{-1} for all measurements (blaze wavelength, 300 nm), with the slit width of the spectrograph being set to 1 mm: this resulted in a spectral resolution of 40 nm. The detector used was a liquid nitrogen cooled CCD array (Princeton Instruments) with UV/antireflection coating operated at 150 K. The CCD-array had a size of 1100×330 pixels. For all measurements described in this work, 2×330 pixels were binned, so that spectra were recorded using 550 data points over the spectral range from 200 to 1200 nm. The use of heat absorbing filters was considered for the TL experiments in order to cut the intense red/IR thermal emission at higher temperatures: however, this would also have resulted in the loss of spectral information below 350 nm, an important region where OSL is concerned. As a consequence, no filters were used in any of the spectral work described here. All spectra have been corrected for wavelength sensitivity of the spectrometer and evaluated between 280 and 900 nm.

For the measurement of TL emission spectra, about 2 mg of each sample was deposited on stainless-steel discs and fixed with silicone oil. A temperature ramp rate of 5 K s^{-1} was used for all measurements, with spectra being recorded using an integration time of 5 s (i.e. giving a temperature resolution of 25 K).

The RL spectra were stimulated by the β and γ emissions from a 3.7 MBq ^{137}Cs-source. The samples (2 mg) were fixed onto an adhesive plastic foil mounted in position directly above the active area of the source, as described by Schilles and Habermann (2000). Using this configuration, RL measurements could only be made at room temperature. The integration time used to record the RL-spectra was 120 s: over this period, the emission intensities were not found to change noticeably.

High-frequency (93 GHz) EPR measurements were carried out in St Andrews at both 300 and 15 K, using a spectrometer similar to that described by Smith *et al* (1998). For measurements using a microwave cavity, only 2 mg of material was required to obtain an optimum cavity filling factor; for spectrometer use in the non-resonant bi-modal reflectance mode, larger sample volumes were required to yield satisfactory signals (namely 75 mg). The specific advantages and problems of high-frequency measurements on quartz have been considered in detail elsewhere (Poolton *et al* 2000).

LM-OSL measurements were carried out at Risø using an automated Risø TLDA 15 system, equipped with an

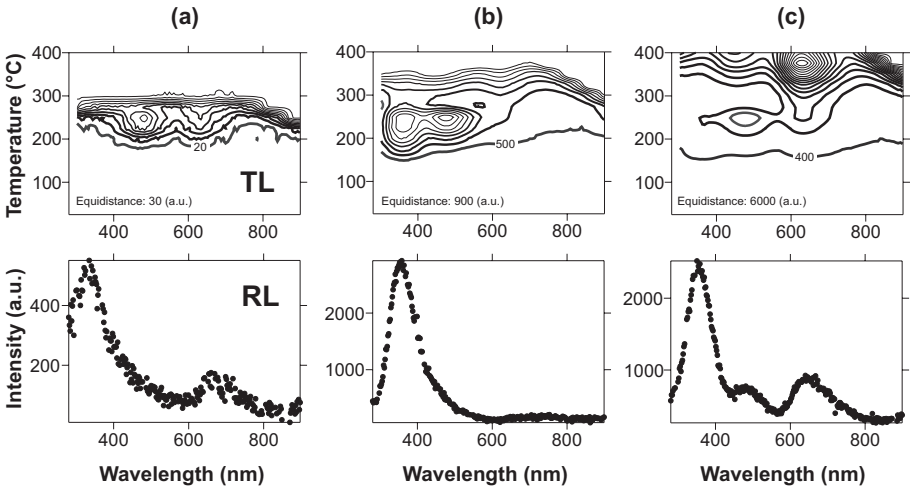


Figure 1. Inter-comparison of the TL emission spectra (top plots) with the RL spectra made at 21 °C (lower curves) for quartz sample A. The spectra are for the natural unheated samples (a), and those that have been heated through the first lattice phase transition, 700 °C (b) and the second phase transition, 1060 °C (c).

array of blue LEDs (peak wavelength 470 nm), delivering up to 50 mW cm^{-2} at the sample (Bøtter-Jensen *et al* 1999). Luminescence was detected using a blue/UV sensitive photomultiplier, prefiltered by Hoya U-340 filters (peak transmission 340 nm, HWHM approximately 40 nm). LM-OSL measurements were carried out by continuously ramping the power from zero to maximum, over a period of typically 6000 s. Measurements were recorded at 160 °C, to avoid retrapping of electrons at donor centres shallower than the OSL traps: such retrapping causes complications in the signal analysis. Full details of the LM-OSL method can be found elsewhere (Bulur 1996, Bulur *et al* 2000).

2.2. Samples

Three different sedimentary quartz samples (referred to as A, B, C) were used for comparison in this study, each one of which was considered to display typical OSL behaviour (i.e. there were no apparent anomalies when dating the material). Sample A (Risø reference number R-992542Q) was a fluvial deposit from the Pechora River, North Russia (age 16 000 years); sample B (R-983031Q) was a modern aeolian deposit from North Jutland, Denmark (age less than 35 years); sample C (R-914807Q) was a marine deposit from North Jutland, age 35 000 years. The measured palaeodoses of A, B and C were 29, 0.1 and 55 Gy, respectively. All samples were subject to the same laboratory preparation and annealing treatment, similar to that described by Bøtter-Jensen *et al* (1995). Briefly, this was (a) HF etching to remove feldspars and other contaminants, (b) prolonged optical bleaching, to remove as much trapped charge as possible, (c) division into a number of sub-aliquots, (d) high-temperature annealing of each sub-aliquot for 1 h in the range 0–1100 °C, (e) γ-irradiation, and (f) measurement. Because of the requirements of the EPR measurements, the sample grains used were in the size range of 63–90 μm, and γ-irradiation was to 3 kGy (significantly above the natural palaeodose). Sample A has been subject to a previous EPR and LM-OSL investigation, as described by Poolton *et al* (2000).

Since the aim of the various spectral measurements was to monitor changes in luminescence sensitivity, emission characteristics, defect populations etc between sub-aliquots annealed at different temperatures, normalization of the signal intensities was provided throughout by means of sample weight.

3. Results and discussion

3.1. Luminescence emission spectra: sample A

The TL and RL emission spectra for three representative aliquots of sample A are shown in figure 1; these are for the natural sediment, and for those that have been annealed past the first and second structural phase transitions. There are several relevant features of the spectra, as outlined below.

(a) Emission bands in both TL and RL appear in the material, peaking at 360, 470 and 630 nm. This indicates that the emission properties of the quartz are entirely typical (Krbetschek *et al* 1997).

(b) The principal change occurring in both the RL and TL spectra after annealing material beyond the first phase transition, is that the UV (360 nm) emission becomes greatly enhanced.

(c) Following annealing beyond the second-phase transition, the red (630 nm) emission band in both RL and TL becomes enhanced.

(d) In all cases, the relative intensity of the UV band is significantly greater in the RL spectra, compared with the TL emission spectra.

The final observation (d) above is strongly indicative that not only thermal quenching effects may play a significant role in the luminescence processes, but that these may be significantly different for the various emission bands. Before considering the *anneal* induced changes in the RL and TL spectra, we wish to first consider in more detail these potential *thermal quenching* effects.

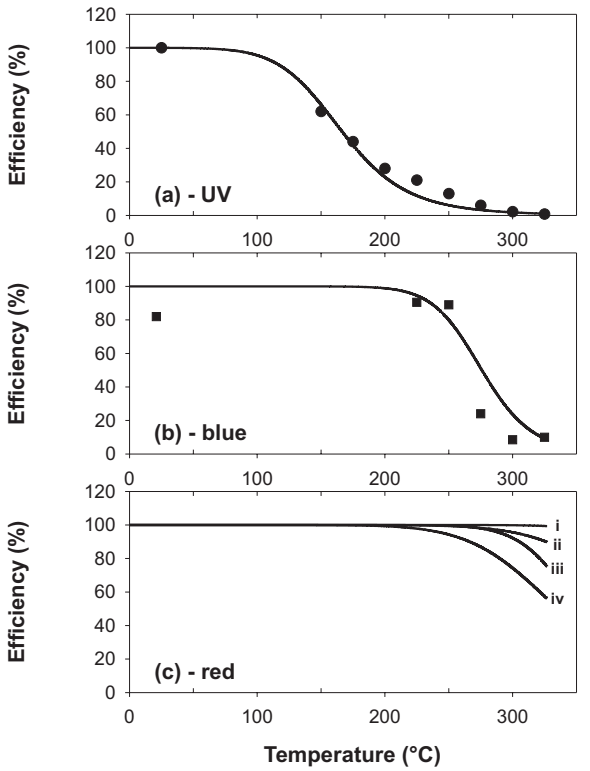


Figure 2. The emission of quartz generally becomes quenched at high temperatures, but this diagram shows that the quenching occurs at different rates for various emission bands. (a) If the red TL is not significantly quenched up to 325 °C, then comparing the 360 and 630 nm TL emission at different measurement temperatures produces the data points as shown, normalized at 21 °C using the RL emission. The theoretical (full) curve uses parameters almost identical with those known for the RL and OSL UV emission, with a quench energy of 0.65 eV. (b) The 470 nm emission evidently is quenched at much higher temperatures than for the 360 nm band (points); the theoretical (full) curve uses a quench energy of 1.32 eV. (c) If the red emission becomes quenched at all, this must occur at temperatures significantly above 300 °C; the theoretical curves drawn here indicate what would happen if the quench energies used in (a), (b) are increased. With $C = 2.8 \times 10^7$, these are $E_q = 0.9$, 1.0 eV (curves iv and ii) and with $C = 1.28 \times 10^7$, these are $E_q = 1.5$, 1.7 eV (curves iii and i).

3.1.1. Thermal quenching of the emission during measurement. Duller *et al* (1995) carried out standard OSL measurements on natural sedimentary quartz at temperatures in the range 20–450 °C, whilst detecting emission in the UV region (filters with peak transmission at 340 nm, HWHM 40 nm). They showed conclusively that the detected emission becomes quenched at elevated temperatures, following the familiar form (Curie 1963):

$$I(T) = 1/[1 + C \exp(-E_q/kT)]. \qquad (1)$$

Here I is the normalized intensity, T is the temperature, C is a constant and E_q is the quench energy. Very good fits of the data to this equation were made, assuming a quenching energy E_q of 0.63 eV, and a C value of 2.8×10^7. These measurements were confirmed by Huntley *et al* (1996) who were able to spectrally identify the emission band being studied, as that of the 370 nm emission. Significantly, these values were almost identical to those obtained earlier by Wintle (1975) who determined the quenching of RL in the UV region, using the parameters $E_q = 0.64$ eV and $C = 2.8 \times 10^7$.

Normally it is very difficult to obtain precise information concerning thermal quenching of specific emission bands from TL measurements, although an indication that thermal quenching is active can be obtained if the TL measurements are made at different temperature ramp rates (e.g. Franklin *et al* 1995). However, we believe that in the particular sample studied in figure 1, it is possible to make a good attempt to obtain a full account of the quenching of all three emission bands from a comparison of the RL and TL data.

We start from the initial premise that there is no observable quenching of the red (630 nm) emission in the temperature region 25–325 °C: this hypothesis derives from the fact that in figure 1(c), the red emission completely dominates the emission at high temperatures, compared with lower temperatures. If correct, this means that if the intensity of the UV (360 nm) emission is compared with that of the red (630 nm), the thermal quenching of the UV band should be directly observable. This is shown diagrammatically in figure 2(a), where the measurements are compared with the theoretical quenching curve obtainable from equation (1), using values very similar to that of Duller *et al* (1995) for the OSL emission (namely $C = 2.8 \times 10^7$ and $E_q = 0.65$ eV). The data of figure 2(a) shows convincingly that the TL from the UV emission is quenching at the same rate as that normally observed in OSL. This observation is significant in two respects. Firstly, it is very good evidence that the OSL and TL processes both feed exactly the same recombination centre involved in the UV (360 nm) emission (this is not easily proven otherwise). Secondly, it shows that our assumption that the red (630 nm) band is not subject to thermal quenching up to 325 °C was valid. In figure 2(a), the normalized value at 20 °C was taken by comparison of the ratio of UV/red from the room temperature RL emission spectrum: since the ratio directly normalizes all the TL measurements, this is a further strong indication that the luminescence recombination processes of the RL and TL are precisely the same.

By carrying out a similar analysis on the blue (470 nm) emission (figure 2(b)), it is immediately clear that the thermal quenching is very different from that of the UV band. Though more scattered, the data is consistent with a thermal quenching process appearing at much higher temperatures: the full curve of figure 2(b) is not intended as a fit, but it uses the same equation (1) (above), and shows that the data is consistent with quenching occurring with the parameters $E_q = 1.32$ eV and $C = 1.28 \times 10^{12}$.

Finally, since both the UV and blue emission bands are subject to thermal quenching, it is also possible that the red emission is too, but at temperatures higher than 325 °C. We can obtain some information about the minimum quenching energy E_q, from figure 2(c). Using the same C parameter as that for the UV band, this would be 1 eV (compared with 0.63 eV for the UV emission), or 1.6 eV (compared with 1.32 eV) if the same C value as the blue band is used.

3.1.2. Anneal induced changes in the RL and TL. In this section, we consider in more detail the changes in RL and TL spectra induced by high-temperature annealing outlined in section 3.1. For sample A, the detailed changes in the intensity

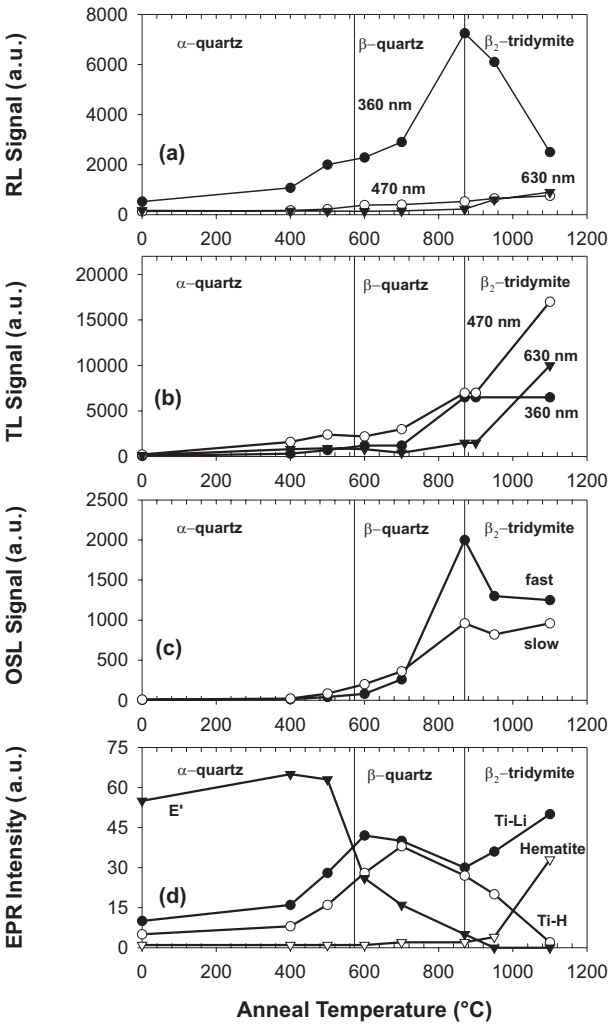


Figure 3. Summary of the anneal induced changes for all the spectral measurements made on sample A. These are for (a) RL (21 °C measurement temperature), (b) TL (225 °C measurement temperature), (c) slow and fast decaying components of the LM-OSL (160 °C measurement temperature) and (d) EPR (300 and 15 K measurement temperatures).

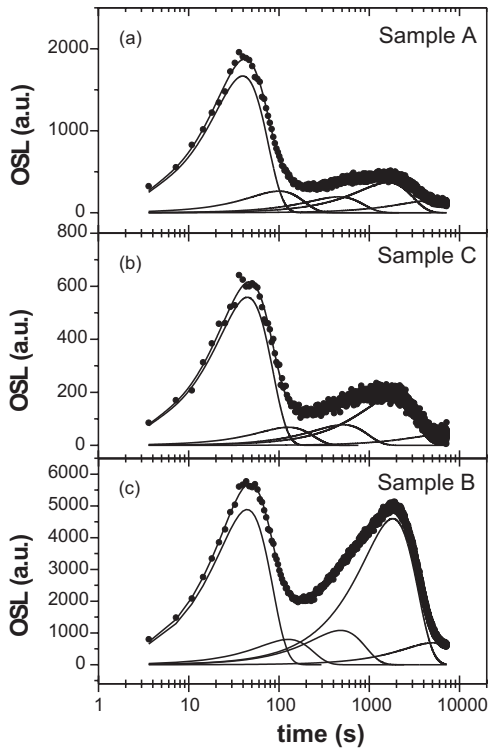


Figure 4. (a)–(c) The LM-OSL curves recorded for samples A, C and B, respectively, annealed at 400 °C; the measured curves (points) can be theoretically accounted for (full curves) in terms of a linear combination of four OSL donor centres with different trap parameters. The features of the spectrum are typical for samples annealed at all temperatures up to 1100 °C, with only minor alteration in the first two components for samples annealed above 950 °C. The anneal-induced changes in the intensity of the fastest and slowest components of sample A are shown in figure 3(c).

of the 360, 470 and 630 nm RL emission bands are shown in figure 3(a). Here it is seen that the dominant emission in all the samples is the UV (360 nm) band; this becomes enhanced (by a factor of 14) mainly in the anneal range 500–870 °C, thereafter again reducing in intensity. The weaker blue (470 nm) band is little affected by the anneal treatment, changing in intensity by only a factor of 3 across the anneal range. The red emission is mainly enhanced for annealing temperatures above 870 °C, for which there is a factor of 6 increase in sensitivity.

For the TL, all three emission bands become enhanced following increased anneal temperature as shown in figure 3(b) (TL recorded at 225 °C). Major increments are shown to occur for the UV and blue bands after annealing between 700 and 870 °C, and for the red emission, this occurs mainly above 950 °C.

The most apparent difference between figures 3(a) and (b), is the relative intensity of the UV band in comparison with the blue and red emissions. From the analysis of section 3.1.1, this is almost certainly due to thermal quenching effects. At the recording temperature (225 °C), the UV, blue and red bands are expected to be suppressed by 90%, 5% and 0%, respectively, compared with measurement at 21 °C (as is the case for RL). Bearing this in mind, the general features of the RL and TL emissions are essentially the same, except that the intensity of the TL UV band is not affected for annealing above 870 °C.

3.2. Linearly modulated OSL

LM-OSL is essentially time-domain excitation spectroscopy: it enables OSL donor defects with different optical capture cross sections to be resolved, by continuously ramping the excitation power from zero to maximum. Typical LM-OSL spectra for samples A, C and B are shown in figures 4(a)–(c) for material that has been annealed at 400 °C: total luminescence is detected in the UV region using filters (340 nm peak, HWHM 40 nm). Fitting the curve using the standard equation (2) requires the presence of four components:

$$L(t) = Ab(t/P)\exp(-(bt^2)/2P). \qquad (2)$$

Here A is the amplitude of the component (proportional to the trapped charge population), P is the period over which the stimulation light intensity is ramped (in this case 7200 s), and $b = \alpha I_0$ where α is the photoionization cross section and I_0 is the maximum intensity of the stimulation light (here

50 mW cm^{-2}). In all cases, the four fitted components lead to peaks at 42 ± 2, 118 ± 15, 485 ± 29 and 1713 ± 106 s: the presence of a weak fifth signal at the longest times (>5000 s) could be indicative of another OSL component, but we are unable to fully identify this signal at present. (As an example, typical b-parameters used for sample C are 3.61, 0.448, 0.027 and 0.0025 for the four peaks, respectively.)

The two LM-OSL components that are of particular significance in figure 4, are the first and last. The first, 'fast decaying' signal is the main component used in normal OSL dosimetry. However, although the intensity appears large, the integrated photon count $\int L(t)\,\mathrm{d}t$ is small in comparison with the total, indicating that there are in fact relatively very few of these particular donor defects present. The component with the largest integral $\int L(t)\,\mathrm{d}t$ is that which is depleted last, the 'slow decaying' trap. This is particularly clear for sample B (figure 4(c)).

For all the variously annealed samples, the b-fitting parameters used for the LM-OSL components remained essentially unchanged, except for a minor alteration in the 'fast' signal following annealing above 950 °C. For the purposes of this work, the actual parameters used (and their meaning) are not important, except for the amplitude of the signals: how these behave with anneal temperature are shown in figure 3(c) for sample A for the fast and slow components respectively. Comparison of these signals with the RL, TL and EPR is discussed in section 3.4.

3.3. EPR spectra: sample A

The EPR spectra obtained from the samples was found to depend on the measurement temperature. Across the annealing range at low measurement temperatures (15 K), the main features were the $[AlO_4]^0$ hole trapping centre, and the $[TiO_4/Li^+]^0$ and $[TiO_4/H^+]^0$ electron trapping centres. At room temperature, the principal signals arose from the oxygen vacancy E′ centre, and from what we take to be magnetically interacting iron (possibly in the form of hematite): this suggestion comes from the near isotropy of the signal, and very broad linewidth (Δ_{pp} = 1000 gauss). The identification of these signals comes from their measured g-values, as presented in table 1, which compare directly with the well documented values given in the literature (example references given). The main advantages for quartz of making the measurements at 93 GHz (rather than the more conventional 9 GHz), is the greater spectrum resolution and sensitivity it provides, and the reduced sample volumes required. The latter are directly comparable with the amounts needed for the various luminescence measurements.

The $[TiO_4/Li^+]^0$ and $[TiO_4/H^+]^0$ electron trapping centres were fully bleachable by exposure to UV/visible light from a standard 75 W Hg–Xe arc lamp, whilst the $[AlO_4]^0$ and E′ hole trapping centres were only partially bleachable. This indicates that the electrons and holes trapped at these centres are optically sensitive, and may therefore play a role in the luminescence processes of the samples. The hematite signal was not changed after exposure to light.

How these various signals change in intensity with anneal treatment of the samples is shown in figure 3(d): since the magnitude of the $[AlO_4]^0$ defect signal is not affected by annealing, for clarity, this is not shown in the figure.

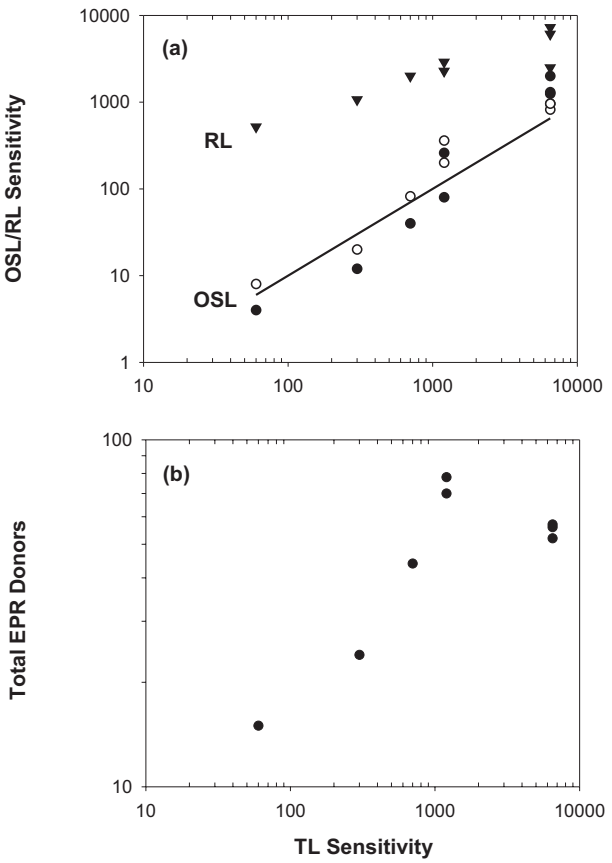


Figure 5. (a) Correlation of the signal intensities of the UV TL emission with the UV detected LM-OSL (open and full circles, for the slow and fast components, respectively), and the UV component of the RL emission. The line indicates the 1:1 relationship. (b) Correlation of the TL sensitivity, with the total number of titanium related donors found in the sample, via EPR.

3.4. Correlation of the spectral properties: sample A

Reference to figure 3 shows that there are many similar features concerning the sensitization of the RL, TL and LM-OSL luminescence processes. Before trying to understand why the sensitization occurs, we seek first to look for consistencies amongst the various features. In figure 5(a), the sensitivity of the TL UV emission is plotted against both the LM-OSL sensitivity (slow and fast components), and the UV emission from the RL. It is immediately apparent that, for material that has been heated up to 870 °C, there is almost exact 1:1 correspondence between the OSL and TL sensitivities for more than two orders of magnitude, strongly indicating that the same processes are involved in both these cases. Significantly, this is not so if the RL emission is compared with that of the TL: here the rate of increase of the RL is less by a factor of 10.

The significant point about RL is that it monitors solely what is happening in the recombination part of the luminescence cycle, whereas both OSL and TL require the existence of electron donor defects as well. For OSL/TL therefore, any sensitivity changes must include the properties of both donors and acceptors. Because we have already provided strong evidence that the recombination part of the TL and OSL cycles are the same as for RL (see section 3.1.2), this means that the annealing process has made the OSL/TL

Table 1. Measured g-values (93 GHz) of the EPR centres present in the quartz studied. References are for the corresponding centres previously reported in the literature.

Defect	g_x	g_y	g_z	Reference
$[AlO_4]^0$	2.0018	2.0082	2.0597	Nuttall and Weil (1981)
$[TiO_4/Li^+]^0$	1.9118	1.9307	1.9782	Isoya *et al* (1988)
$[TiO_4/H^+]^0$	1.9149	1.9307	1.9845	Rinneberg and Weil (1972)
$[TiO_4/Na^+]^0$	1.8988	1.9516	1.9702	Bailey and Weil (1992)
E′	2.00032	2.00051	2.00181	Jani *et al* (1983)
Hematite	1.998	1.998	1.998	Griscom *et al* (1979)

excitation process more sensitive than RL by a factor of 10. The simplest explanation for this would be that the number of donor defects has increased by this amount. Without being drawn into assigning the microstructure of individual OSL and TL donor species, we can say from figure 5(b) that, as monitored by EPR, there is an increase in the number of [Ti–H/Li] donors by a factor of 10, over the required anneal temperature range. We also highlight the point that these paramagnetic donors were found to be optically bleachable, and thus are possibly involved in the luminescence processes.

If the above is good evidence for the (donor) defect creation concept to explain part of the anneal-induced OSL sensitivity increase, we also need to consider this possibility for the recombination part of the cycle (i.e. as monitored purely in RL). Unfortunately, there is no evidence at all from the EPR that acceptor centres are created in this sample by annealing. The dominant recombination centre is the $[AlO_4]^0$ defect, and the population of this was found to be invariant with the annealing, up to 1100 °C. The RL measurements show that the dominant recombination band in these samples is the 360 nm UV emission. Although there has been some debate as to the acceptor defects involved in the 360 nm and blue 470 nm emission bands (e.g. Yang and McKeever (1990) attributed these to the $[H_3O_4]^0$ and $[AlO_4]^0$ defects, respectively—both very similar centres), other convincing evidence was presented by Martini *et al* (1995) who linked more conclusively the UV 380 nm emission with that of the $[AlO_4]^0$ centre. Our results are consistent with this attribution; furthermore, we do not observe the $[H_3O_4]^0$ centre in the EPR from our samples. It is very possible that, since the UV band is so strongly thermally quenched compared with other emission bands (see figure 2), its significance in connection with $[AlO_4]^0$ may have previously been overlooked.

If there is no evidence to support the view that the RL (and TL, OSL) is enhanced due to the creation of recombination centres, we still must consider the possibility that E′ centres act as competitive traps in the recombination process: as previously noted by Poolton *et al* (2000), these defects become annealed out of the samples over the anneal temperature range 500–870 °C, just as the luminescence features become enhanced (as in figure 6).

The features of figure 6 show the sensitivity increase of the UV band, mainly in the anneal temperature range 400–870 °C, but there are also enhancements of the blue and red emissions in this range (figure 3). There is no evidence from the emission spectra indicating the *loss* of luminescence which could be associated with the destruction of E′, at least in the range monitored, 280–900 nm. As a consequence, we can exclude the possibility that the E′

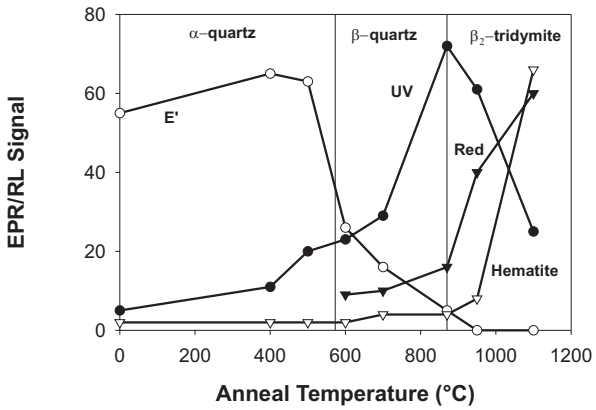


Figure 6. The oxygen vacancy E′ centres are thought to act in competition with the main UV RL (and OSL, TL) emission of the sample, emitting either non-radiatively, or out of the spectral range 280–900 nm. As these become annealed, the luminescence efficiency of the UV band increases. For annealing beyond the second phase transition, there is major disruption of the lattice, indicated by the appearance of a hematite signal in EPR (see text for possible mechanism). This lattice disruption is coincident with the strengthening of the red emission and, because of competition, a related decrease in the UV emission.

contributes *radiatively* to the luminescence in this spectral region. The best evidence that E′ is directly linked to a luminescence feature comes from inter-comparative EPR, optical absorption and luminescence measurements made by Jones and Embree (1976) who associate E′ in crystalline quartz with the 260 nm emission. This wavelength region is close to the limit of our spectral measurement possibilities: although we do see some evidence for emission in the range 240–280 nm, this is not always erased following samples annealing above 700 °C (when the E′ centres disappear). On the other hand, Paccioni *et al* (1998) show that theoretically, E′ will act as a non-radiative recombination centre in silica. For our purposes, identifying which of these explanations is correct is not important: the significant point is that previous work has provided evidence to suggest that E′ acts as a recombination centre, emitting either non-radiatively, or outside the spectral range of our instruments. We find no evidence to contradict this.

The spectral measurements presented in this work, therefore, provide further support for the concept that E′ acts in competition with the emission bands in the near UV and visible regions, so that its thermal removal from the samples leads to an enhancement in the luminescence sensitivity. This enhancement is primarily associated with the UV (360 nm) emission, possibly indicative of preferential pairing of the centres.

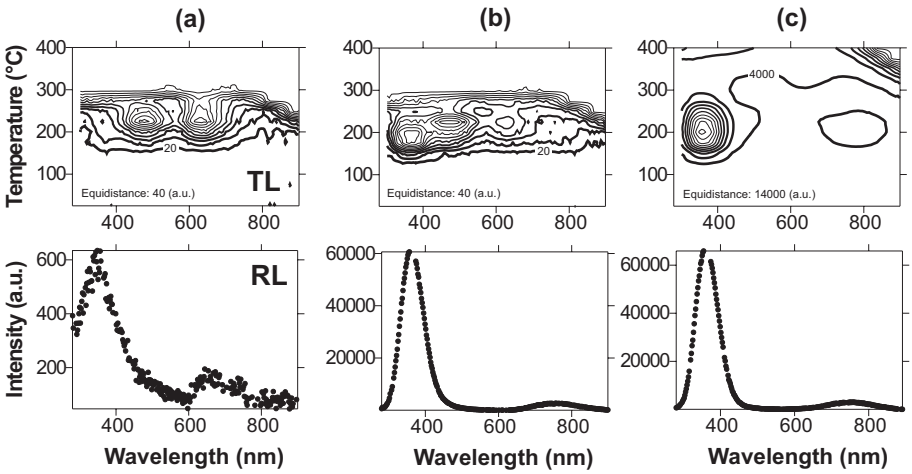


Figure 7. Inter-comparison of the TL emission spectra (top plots) with the RL spectra made at 21 °C (lower curves) for quartz sample B. The spectra are for the natural unheated samples (a), and those that have been heated through the first lattice phase transition, 700 °C (b) and the second phase transition, 1060 °C (c). The significant feature of this figure is that the emission of this sample (both RL and TL) is completely dominated by the UV bands: the small signal at around 720 nm is due entirely to second-order 360 nm emission.

Finally in this section, we comment on the feature of figure 6 that, for annealing of the samples above the second quartz phase transition, the red RL emission of the samples becomes enhanced at the same time that the UV emission is reduced. Again, this is interpreted as arising from competition in recombination between the red and UV emission bands. The defect responsible for the red band is unknown, but the increase in its intensity is directly coincident with the appearance of the hematite EPR signal. The latter is probably indicative of major changes in the crystal lattice beginning to occur, since the hematite signal can only appear by the accumulation of iron into clusters, induced by enhanced mobility of the ions.

3.5. Spectral properties of quartz samples B and C

Even though the quartz material used came from very different geographical regions, many properties of the TL, OSL and EPR characteristics were essentially the same, particularly for the unheated material. After annealing, however, some of the features of the samples did vary, and we seek to highlight such differences in this section.

The TL and RL emission spectra of samples B and C were identical to those of sample A for both the natural samples, and those that had been annealed up to 700 °C. Annealing sample B to higher temperatures (1060 °C) resulted in both TL and RL emission spectra being totally dominated by the UV (360 nm) emission, as shown in figure 7. This contrasts with samples C and A (figure 1), where high-temperature annealing results in the TL being dominated by the *red* (630 nm) emission—which is also strong in the RL.

For all three samples, the oxygen vacancy E′ EPR centre was found to become annealed out of the samples at around the first phase transition (573 °C), close to the point at which the dominant OSL sensitivity increases commence. This again confirms the idea that E′ acts as a competitive, non-radiative recombination centre. For sample C, the electron donor centres $[TiO_4/Li^+]^0$ and $[TiO_4/H^+]^0$ appear (as for samples A and B) but there is also a third defect present (figure 8(a)), identified from its g-values as $[TiO_4/Na^+]^0$: see table 1 for the measured g-parameters. The anneal induced behaviour of both $[TiO_4/Li^+]^0$ and $[TiO_4/H^+]^0$ centres was as described for sample A (and B), but the new $[TiO_4/Na^+]^0$ centre was

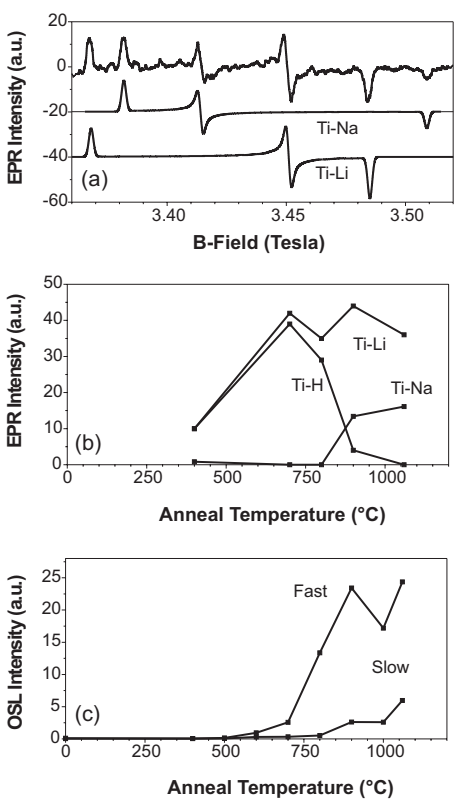


Figure 8. Anneal-induced changes in the properties of quartz sample C following γ-irradiation. (a) Low-temperature EPR spectrum (top) observed in high-temperature (1060 °C) material. The simulated curves for T–Na and Ti–Li centres are also shown, with the measured g-parameters given in table 1. Linewidth used = 22 G (so no hyperfine splittings are observable). (b) Anneal-induced behaviour of all three Ti-related defects. (c) Anneal-induced changes in the intensity of the slow and fast decaying OSL components.

found only to appear in significant quantities for annealing above the second phase transition at 870 °C. Comparison can be drawn between the anneal induced changes of all three Ti centres (figure 8(b)), and the fast and slow components of the LM-OSL (figure 8(c)): these are found to be almost identical with that for the LM-OSL of sample A (figure 3(c)), except for a change in the relative intensities of the components.

As a final comment, we note that anneal-induced sensitivity changes in the quartz should be almost universally observable. This comment arises, since we have shown that the changes are driven by a combination of both oxygen vacancy centres and aluminium impurities, and these are nearly always present in unheated quartz.

4. Conclusions

The general conclusion of this work is that multi-spectroscopic approaches to the analysis of luminescence phenomena in quartz provide substantially improved understanding of the emission processes, unobtainable by using any one method in isolation. The specific conclusions for the annealed quartz measured in the study are:

(a) The emission bands commonly observed in TL from quartz are subject to significant thermal quenching. The quenching energy of the TL for the UV (360 nm) emission was found to be 0.65 eV, and 1.32 eV for the blue (470 nm) luminescence. The common red (630 nm) emission was found not to significantly quench for temperatures up to 325 °C, making an absolute lower figure for any quench energy to be 1 eV.

(b) The recombination processes in both RL and TL are essentially the same, employing identical recombination centres. The defects responsible for the red and blue bands compete with one another for recombining electrons.

(c) Strong evidence exists to show that E′ oxygen vacancies are important recombination centres acting in competition mainly with the defects responsible for the UV emission (and to a lesser extent, the blue and red emission). No evidence was found to suggest that E′ contributes radiatively to the emission processes, within the wavelength range 280–900 nm.

(d) E′ centres become annealed out of the samples when heated in the temperature range 500–870 °C (the exact temperature being slightly sample dependent). The removal of these recombination centres enhances the luminescence efficiency in the wavelength range 280–900 nm.

(e) Annealing samples beyond the β-quartz–β_2 tridymite phase transition at 870 °C leads to significantly enhanced ion mobility, as evidenced by the appearance in all samples studied, of EPR signals attributed to magnetically interacting iron particles. In some samples, annealing at such temperatures also leads to the creation of $[TiO_4/Na^+]^0$ centres, and/or to a greatly enhanced red emission.

Acknowledgments

NRJP is grateful to the Royal Society for the provision of funds from the European Science Exchange Programme, to facilitate the inter-laboratory collaboration of this investigation. The work is funded in the UK by the Engineering and Physical Science Research Council (EPSRC grant no GR/L49628) and in Denmark by the Danish National Laboratory, Risø and by Aarhus University.

References

Aitken M J 1985 *Thermoluminescence Dating* (London: Academic)
——1998 *An Introduction to Optical Dating: the Dating of Quaternary Sediments by the use of Photon-stimulated Luminescence* (Oxford: Oxford University Press)
Bailey P and Weil J A 1992 The EPR spectral parameters and dynamic properties of the centre $[TiO_4/Na]^0_A$ in *X*-irradiated α-quartz *J. Phys. Chem. Solids* **53** 309–18
Bøtter-Jensen L, Agersnap Larsen N, Mejdahl V, Poolton N R J, Morris M F and McKeever S W S 1995 Luminescence sensitivity changes in quartz as a result of annealing *Radiat. Meas.* **24** 535–41
Bøtter-Jensen L, Duller G A T, Murray A S and Banerjee D 1999 Blue light emitting diodes for optical stimulation of quartz in retrospective dosimetry and dating *Radiat. Prot. Dosim.* **84** 335–40
Bulur E 1996 An alternative technique for optically stimulated luminescence experiment *Radiat. Meas.* **26** 701–9
Bulur E, Bøtter-Jensen L and Murray A S 2000 Optically stimulated luminescence from quartz measured using linear modulation technique *Radiat. Meas.* **32** 407–11
Curie D 1963 *Luminescence in Crystals* (New York: Wiley)
Duller G A T, Bøtter-Jensen L and Poolton N R J 1995 Stimulation of mineral-specific luminescence from multi-mineral samples *Radiat. Meas.* **24** 87–93
Franklin A D, Prescott J R and Scholefield R B 1995 The mechanism of thermoluminescence in an Australian sedimentary quartz *J. Lumin.* **63** 317–26
Griscom D L, Friebele E J and Shinn D B 1979 Ferromagnetic resonance of spherical particles of α-iron precipitated in fused quartz *J. Appl. Phys.* **50** 2402–4
Huntley D J, Godfrey-Smith D I and Haskell E H 1991 Light induced emission spectra from some quartz and feldspars *Nucl. Tracks Radiat. Meas.* **18** 127–31
Huntley D J, Short M A and Dunphy K 1996 Deep traps in quartz and their use for optical dating *Can. J. Phys.* **74** 81–91
Isoya J, Tennant W C and Weil J A 1988 Electron paramagnetic resonance of the TiO_4/Li centre in crystalline quartz *J. Magn. Reson.* **79** 90–8
Jani M G, Bossoli R B and Halliburton L E 1983 Further characterization of the E'_1 centre in crystalline SiO_2 *Phys. Rev.* B **27** 2285–93
Jones C E and Embree D 1976 Correlation of the 4.77–4.78 eV luminescence band in silica with the oxygen vacancy *J. Appl. Phys.* **47** 5365–71
Krbetschek M R, Götze J, Dietrich A and Trautmann T 1997 Spectral information from minerals relevant for luminescence dating *Radiat. Meas.* **27** 695–748
Lee H K and Schwarcz H P 1994 Criteria for complete zeroing of ESR signals during faulting of the San Gabriel fault zone, Southern California *Tectonophysics* **235** 317–37
Marazuev Yu A, Brik A B and Degoda V Ya 1995 Radioluminescent dosimetry of α-quartz *Radiat. Meas.* **24** 565–9
Martini M, Paleari A, Spinologo G and Vedda A 1995 Role of $[AlO_4]^0$ centres in the 380 nm thermoluminescence of quartz *Phys. Rev.* B **52** 138–42
Nuttall R H D and Weil J A 1981 The magnetic properties of the oxygen-hole aluminium centre in crystalline SiO_2. I. $[AlO_4]^0$ *Can. J. Phys.* **59** 1696–708
Paccioni G, Ieranò G and Márquez A M 1998 Optical absorption and nonradiative decay mechanism of E′ in silica *Phys. Rev. Lett.* **81** 377–80

Poolton N R J, Smith G M, Riedi P C, Bulur E, Bøtter-Jensen L, Murray A S and Adrian M 2000 Luminescence sensitivity changes in natural quartz induced by high temperature annealing: a high frequency EPR and OSL study *J. Phys. D: Appl. Phys.* **33** 1007–17

Rieser U, Habermann J and Wagner G A 1999 Luminescence dating: a new high sensitivity TL/OSL emission spectrometer *Quaternary Geochronol.* **18** 311–15

Rink W J, Rendell H, Marseglia E A, Luff B J and Townsend P D 1993 Thermoluminescence spectra of igneous quartz and hydrothermal vein quartz *Phys. Chem. Minerals* **20** 353–61

Rinneberg H and Weil J A 1972 EPR studies of Ti^{3+}–H^{+} centres in X-irradiated α-quartz *J. Chem. Phys.* **56** 2019–28

Schilles T and Habermann J 2000 Radioluminescence dating: the IR emission of feldspar *Radiat. Meas.* **32** 679–83

Smith G M, Lesurf J C G, Mitchell R H and Riedi P C 1998 Quasi-optical cw mm-wave electron spin resonance spectrometer *Rev. Sci. Instrum.* **69** 3924–37

Wintle A G 1975 Thermal quenching of thermoluminescence in quartz *Geophys. J. R. Astron. Soc.* **41** 107–13

Yang X H and McKeever S W S 1990 The predose effect in crystalline quartz *J. Phys. D: Appl. Phys.* **23** 237–44